

Shank3 mutant mice display autistic-like behaviours and striatal dysfunction

João Peça^{1,2*}, Cátia Feliciano^{1,3*}, Jonathan T. Ting¹, Wenting Wang¹, Michael F. Wells¹, Talaigair N. Venkatraman⁴, Christopher D. Lascola^{1,4}, Zhanyan Fu^{1,5,6} & Guoping Feng^{1,6,7}

Autism spectrum disorders (ASDs) comprise a range of disorders that share a core of neurobehavioural deficits characterized by widespread abnormalities in social interactions, deficits in communication as well as restricted interests and repetitive behaviours. The neurological basis and circuitry mechanisms underlying these abnormal behaviours are poorly understood. SHANK3 is a postsynaptic protein, whose disruption at the genetic level is thought to be responsible for the development of 22q13 deletion syndrome (Phelan–McDermid syndrome) and other non-syndromic ASDs. Here we show that mice with *Shank3* gene deletions exhibit self-injurious repetitive grooming and deficits in social interaction. Cellular, electrophysiological and biochemical analyses uncovered defects at striatal synapses and cortico-striatal circuits in *Shank3* mutant mice. Our findings demonstrate a critical role for SHANK3 in the normal development of neuronal connectivity and establish causality between a disruption in the *Shank3* gene and the genesis of autistic-like behaviours in mice.

Autism and autism spectrum disorders (ASDs) are neurodevelopmental disorders diagnosed based on a triad of criteria: deficits in communication, impaired social interaction, and repetitive or restricted interests and behaviours¹. ASDs are highly heritable disorders with concordance rates as high as 90% for monozygotic twins². Recent genetic and genomic studies have identified a large number of candidate genes for ASDs³, many of which encode synaptic proteins^{4–6}, indicating synaptic dysfunction may have a critical role in ASDs^{7,8}. One of the most promising ASD candidate genes is *Shank3*, which codes for a key postsynaptic density (PSD) protein at glutamatergic synapses. Disruption of *Shank3* is thought to be the cause of core neurodevelopmental and neurobehavioural deficits in the 22q13 deletion syndrome (Phelan–McDermid syndrome), an autism spectrum disorder^{9–11}. Furthermore, recent genetic screens have identified several mutations/rare variants of the *Shank3* gene in ASD patients outside of diagnosed 22q13 deletion syndrome^{12,13}.

The Shank family of proteins (SHANK1–3) directly bind SAPAP (also known as DLGAP) to form the PSD-95–SAPAP–SHANK complex^{14,15} (PSD-95 is also known as DLG4). This core of proteins is thought to function as a scaffold, orchestrating the assembly of the macromolecular postsynaptic signalling complex at glutamatergic synapses. Currently, however, little is known about the *in vivo* function of SHANK3 at the synapse and how a disruption of *Shank3* may contribute to ASDs. Here we demonstrate that genetic disruption of *Shank3* in mice leads to compulsive/repetitive behaviour and impaired social interaction, resembling two of the cardinal features of ASDs. Biochemical, morphological and electrophysiological studies revealed synaptic dysfunction at cortico-striatal synapses, part of the neural circuits strongly implicated as dysfunctional in ASDs. Our studies provide a synaptic and circuitry mechanism underlying *Shank3* disruption and ASD-like behaviours.

Shank3B^{-/-} mice display repetitive grooming

The *Shank3* gene codes for large proteins with multiple protein–protein interaction domains (Fig. 1a). We generated two different

alleles of SHANK3 mutant mice. In *Shank3A* mutant mice, we targeted a portion of the gene encoding the ankyrin repeats (Supplementary Fig. 1b). This resulted in a complete elimination of SHANK3_α, the longest SHANK3 isoform (Fig. 1b). However, the other two isoforms were not affected (here named SHANK3_β and SHANK3_γ). In *Shank3B* mutants, we targeted the fragment encoding the PDZ domain (Supplementary Fig. 1c). This led to the complete elimination of both SHANK3_α and SHANK3_β isoforms and a significant reduction of the putative SHANK3_γ isoform at the PSD (−42.12% ± 9.27% of control, *n* = 3, *P* < 0.05) (Fig. 1b). Our analysis is mainly focused on the *Shank3B*^{-/-} mutants due to their more pronounced behavioural and physiological defects.

We used mice with a hybrid genetic background to avoid the potential contribution to behavioural phenotypes of homozygous genetic variants on a pure inbred background^{7,16}. Initially, F1 hybrids from heterozygous × heterozygous matings were generated and homozygous mice were born at an expected Mendelian rate. However, homozygous knockout mice from this type of mating are smaller than their wild-type littermates, presumably due to inadequate competition for resources during early postnatal days leading to different developmental trajectories. We postulated that this size difference would influence our behavioural tests. To alleviate this confound, heterozygous animals were crossed in direct brother–sister matings for five generations from which we derived F5 isogenic hybrids in a mixed background. These isogenic animals were then used to generate time-mated homozygous × homozygous breeding pairs to obtain wild-type and mutant animals used in the experiments. F5 *Shank3A* and F5 *Shank3B* knockouts from these matings are reared to weaning age with body weights similar to those from F5 control animals.

Shank3B^{-/-} mice did not display any gross anatomical or histological brain abnormality, but on rare occasions exhibited seizures during handling in routine husbandry procedures. However, spontaneous seizures were never observed. By the age of 3–6 months, *Shank3B*^{-/-}

¹Department of Neurobiology, Duke University Medical Center, Durham, North Carolina 27710, USA. ²PhD Programme in Biomedicine and Experimental Biology (BEB), Center for Neuroscience and Cell Biology, University of Coimbra, Coimbra, Portugal. ³Gulbenkian PhD Programme in Biomedicine, Gulbenkian Science Institute, 2781-901 Oeiras, Portugal. ⁴Department of Radiology, and Brain Imaging and Analysis Center, Duke University Medical Center, Durham, North Carolina 27710, USA. ⁵Department of Psychiatry and Behavioral Science, Duke University Medical Center, Durham, North Carolina 27710, USA. ⁶McGovern Institute for Brain Research, Department of Brain and Cognitive Sciences, Massachusetts Institute of Technology, Cambridge, Massachusetts 02139, USA. ⁷Stanley Center for Psychiatric Research, Broad Institute, Cambridge, Massachusetts 02142, USA.

*These authors contributed equally to this work.

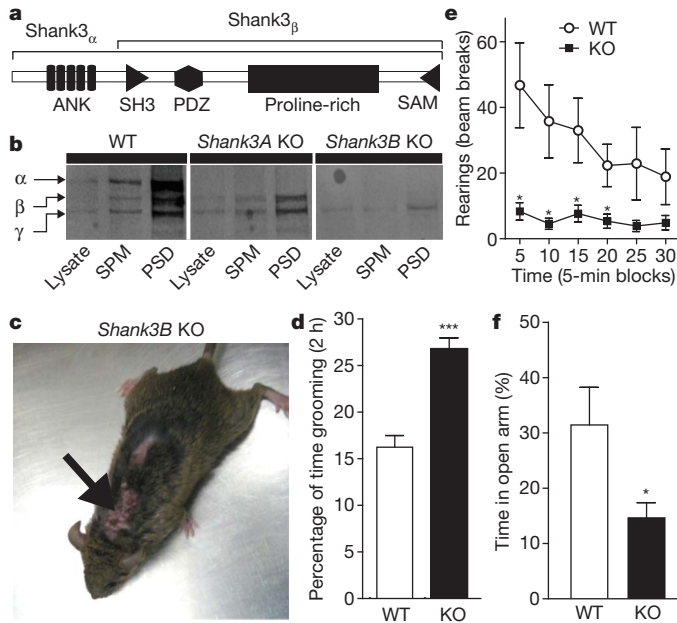


Figure 1 | Excessive grooming, skin lesions and anxiety-like behaviour in *Shank3B*^{-/-} mice. **a**, SHANK3 protein structure. **b**, Western blot showing a pan-SHANK3 antibody staining in brain lysate, synaptosomal plasma membrane (SPM) and 2× Triton X-100-washed PSD (PSD) fraction in wild-type (WT), *Shank3A*^{-/-} and *Shank3B*^{-/-} mice. **c**, Four-month-old *Shank3B*^{-/-} mice display neck and head lesions (arrows). **d**, Pre-lesion *Shank3B*^{-/-} (KO) mice spent more time in self-grooming than WT. **e**, In the open field test, *Shank3B*^{-/-} mice, when compared to controls, display decreased rearing activity. **f**, In the zero maze test, *Shank3B*^{-/-} mice spent less time in the open area than wild-type controls. **P* < 0.05, ****P* < 0.001, two-tailed *t*-test for **d** and **f**, two-way repeated measures ANOVA with post hoc two-tailed *t*-test for **e**; all data are presented as means ± s.e.m. from 6–9 mice per genotype.

mice developed pronounced skin lesions with varying degrees of phenotypical penetrance: approximately 35% in the general holding colony (Fishers exact test, *P* < 0.0001), and 100% in mating females that have produced 4–6 litters. The lesions tend to appear first on the back of the neck or on the face (Fig. 1c) and usually progressed bilaterally to cover large areas of the body. The lesions were self-inflicted, as they were present in animals socially isolated at weaning age, and not due to excessive allogrooming, as no lesions were found in wild-type or *Shank3B*^{+/-} mice housed from birth with *Shank3B*^{-/-} animals. Furthermore, 24 h videotaping in pre-lesion animals revealed that *Shank3B*^{-/-} mice showed an increase in time spent grooming when compared to wild-type controls (Fig. 1d). These observations indicate that *Shank3B*^{-/-} mice display excessive grooming and self-injurious behaviour.

We characterized the animals further in a battery of behavioural tests. In the rotarod motor test, *Shank3B*^{-/-} and control animals performed at similar levels (Supplementary Fig. 2). In the open field test, when compared to controls, *Shank3B*^{-/-} mice showed similar levels of activity and thigmotaxis (Supplementary Fig. 2). However, rearing, which is a form of vertical exploration considered to be anxiogenic for mice, was significantly reduced in the mutants (Fig. 1e). In the elevated zero maze, the *Shank3B*^{-/-} mice spent less time exploring the open arms of the maze versus the closed arms (Fig. 1f). In the light–dark emergence test, the *Shank3B*^{-/-} mice displayed an increased latency to cross into the brightly lit area, although the time spent in each side of the box was similar between mutant animals and controls (Supplementary Fig. 2). Thus, the *Shank3B*^{-/-} mice display an anxiety-like behaviour and excessive, self-injurious grooming. In contrast, *Shank3A*^{-/-} mice displayed no lesions or anxiety-like behaviour (Supplementary Fig. 3).

Social interaction deficits in *Shank3B*^{-/-} mice

Deficits in social interaction are the most recognizable manifestation of autistic behaviours in humans. We used a modified version of a three-chamber social arena¹⁷ to probe animals for their voluntary initiation of social interaction and their ability to discriminate social novelty. Initially, the test animal was left to explore and initiate social contact with a partner ('Stranger 1') held inside a wired cage or an identical but empty wired cage ('Empty cage'). In this test, the *Shank3B*^{-/-} mice displayed dysfunctional social interaction behaviour, as measured by observing both time spent in the compartment containing the social partner (Fig. 2a, b) or in close interaction (Fig. 2d). Notably, *Shank3B*^{-/-} mice exhibited a clear preference for interacting with the empty cage rather than with the social partner (Fig. 2a, d). In a subsequent trial, a novel social partner ('Stranger 2') was introduced into the previously empty wired cage. Wild-type mice displayed a preference for the novel animal, as shown by the increase in time spent in the compartment containing 'Stranger 2'. The *Shank3B*^{-/-} mutants markedly spent more time in the centre chamber (Fig. 2c) and a reduced amount of time closely interacting with either social partner (Fig. 2e). In an identical test, the *Shank3A*^{-/-} mice displayed normal initiation of social interaction, but perturbed recognition of social novelty (Supplementary Fig. 4).

Additionally, in an open arena test, freely interacting dyadic pairs of wild-type–*Shank3B*^{-/-} mice displayed less time spent in reciprocal interaction, a lower frequency of nose-to-nose interaction and anogenital sniffing when compared to wild-type–wild-type pairs (Supplementary Fig. 5). Thus, data from both social interaction tests indicate that *Shank3B*^{-/-} mice display abnormal social interaction as well as deficits in discriminating social novelty.

In our breeding scheme, *Shank3B*^{-/-} mice and wild-type mice were nurtured by *Shank3B*^{-/-} and wild-type dams, respectively. To assess the impact of maternal rearing on the observed sociability defects, we performed time-mated cross-fostering of *Shank3B*^{-/-} mice and controls. Cross-fostering of *Shank3B*^{-/-} neonatal pups with wild-type dams (KO_{ct}) revealed qualitatively equivalent social defects in the mutant mice as compared to those observed in mutant mice nurtured by *Shank3B*^{-/-} dams. Additionally, rearing wild-type neonatal pups by *Shank3B*^{-/-} dams (WT_{ct}) did not perturb normal sociability in wild-type animals (Supplementary Fig. 6). These data further indicate a genetic origin of the abnormal social behaviours in the *Shank3* mutant mice.

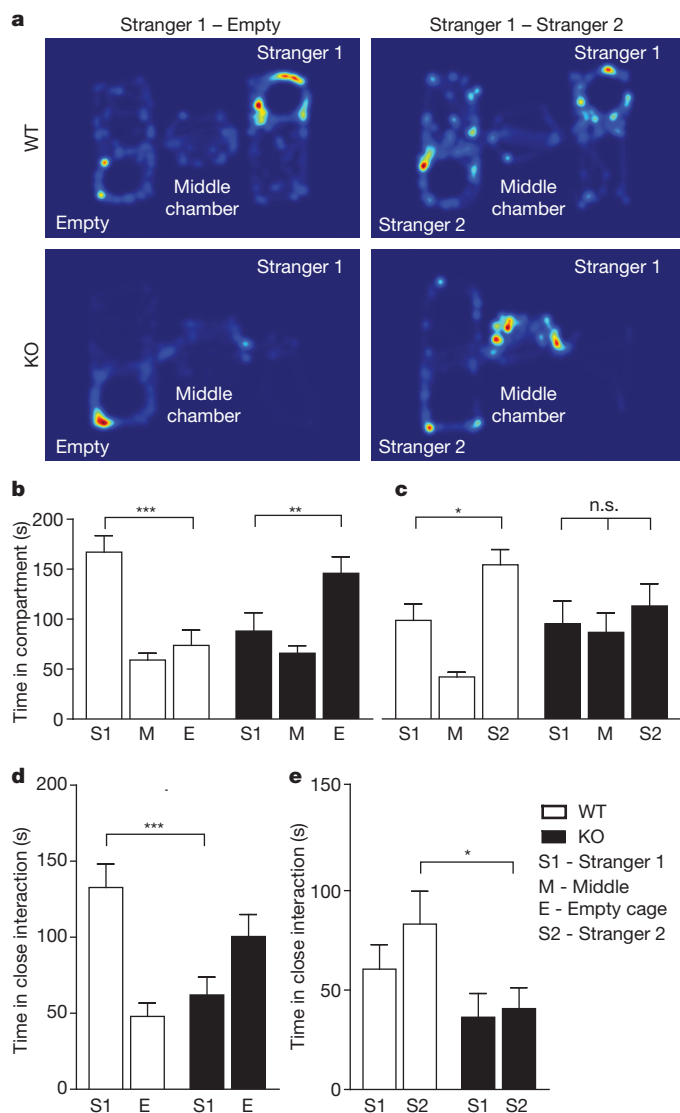
Altered PSD composition in the striatum

The basal ganglia are one of the brain regions implicated as dysfunctional in ASD. The repetitive/compulsive grooming behaviour in *Shank3B*^{-/-} mice also suggests defects in cortico-striatal function. Furthermore, *Shank3*, but not *Shank1* or *Shank2*, is highly expressed in the striatum (Fig. 3a) (Supplementary Fig. 7 and Supplementary Table 1). Therefore, we focused our analyses on striatal neurons and cortico-striatal synapses.

Shank family members have been proposed as key regulators of the PSD at glutamatergic synapses¹⁸. To determine how the disruption of *Shank3* may affect the PSD protein network, we used biochemically purified PSDs from the striatum of wild-type and *Shank3B*^{-/-} mice and performed semiquantitative western blotting for several scaffolding proteins (Fig. 3b) and glutamate receptor subunits (Fig. 3c). At the PSD level, we observed reduced levels of SAPAP3, Homer-1b/c and PSD-93 (also known as HOMER1 and DLG2, respectively; Fig. 3b) as well as a reduction in the glutamate receptor subunits GluR2, NR2A and NR2B (also known as GRIA2, GRIN2A and GRIN2B, respectively; Fig. 3c). These results suggest an altered molecular composition of postsynaptic machinery in the striatum and a possible disruption of glutamatergic signalling.

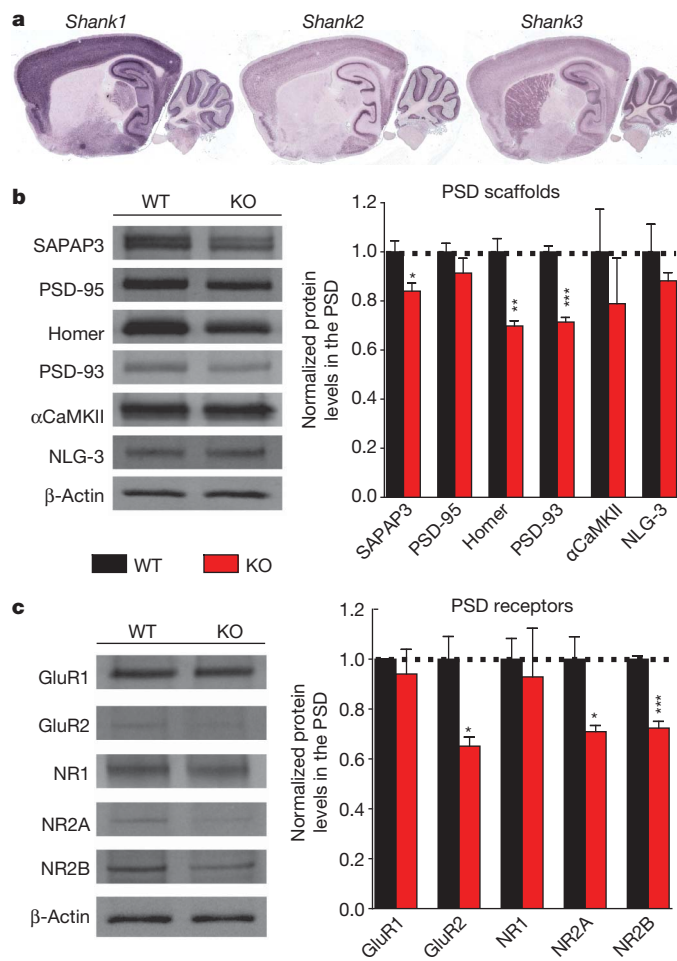
Morphological defects of medium spiny neurons

To test whether disruption of SHANK3 affects neuronal morphology, we traced Golgi-stained striatal medium spiny neurons (MSNs) and



their dendrites to investigate the cellular morphology and complexity of these cells. Sholl analysis revealed neuronal hypertrophy as measured by an increase in complexity of dendritic arborizations (Fig. 4a), total dendritic length (Fig. 4b) and also an increase in surface area (Fig. 4c) in *Shank3B*^{-/-} MSNs.

Next, we performed patch-assisted Lucifer Yellow cell filling of MSNs and measured spine density in control and *Shank3B*^{-/-} mice. *Shank3B*^{-/-} mice displayed a significant reduction in spine density (Fig. 4d, e). We did not observe significant changes in spine length or head diameter; however, the neck width of *Shank3B*^{-/-} MSN spines was slightly larger than that of controls (Supplementary Fig. 8).



Finally we analysed PSD morphology by electron microscopy (Fig. 4f). We found a significant reduction in mean thickness (Fig. 4g) of PSDs from *Shank3B*^{-/-} mice relative to controls. Additionally, PSD length was also significantly reduced in the *Shank3B*^{-/-} mice (Fig. 4h). Taken together, these results highlight a critical *in vivo* role for *Shank3* in the normal development of medium spiny neurons and striatal glutamatergic synapses.

Striatal hypertrophy in *Shank3B*^{-/-} mice

Even though there is no clear correlation between brain size or neuronal hypertrophy specifically for *Shank3* disruptions in humans, a potential link between enlarged brain size, neuronal hypertrophy and autism has been suggested previously¹⁹. In particular, increased caudate volume in autism patients has been proposed to be linked to repetitive behaviours^{20,21}. We measured striatal volume using three-dimensional magnetic resonance imaging in the intact brain of *Shank3B*^{-/-} and control mice. We found that there was no significant difference in overall brain size between the genotypes. However, measurement of caudate volume in the same animals revealed a small but

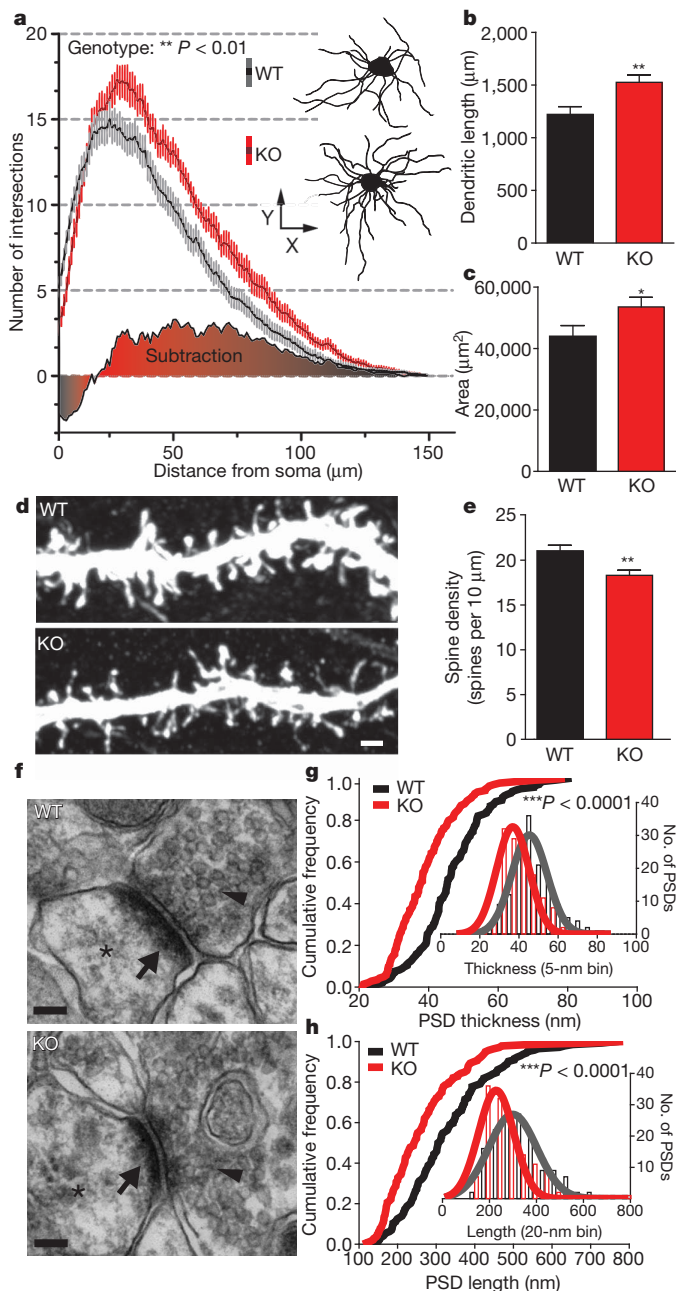


Figure 4 | Morphological and ultrastructural neuronal abnormalities in *Shank3B*^{-/-} mice. **a**, Sholl analysis reveals an increased neuronal complexity of *Shank3B*^{-/-} MSNs (red) when compared to MSNs from wild-type mice (grey); example neurons are shown as insets (top, WT-; bottom, KO-). **b**, **c**, MSNs from *Shank3B*^{-/-} mice show an increase in total dendritic length (**b**) and surface area (**c**) when compared to controls. **d**, Representative confocal stacks of dye-filled MSNs from KO and WT mice; scale bar, 1 µm. **e**, Spine density in MSNs from *Shank3B*^{-/-} mice is lower than that of wild-type MSNs. **f**, Examples of electron micrographs depicting the synaptic contacts with presynaptic vesicles (arrowheads), postsynaptic densities (arrow) and dendritic spine (asterisk); scale bar, 100 nm. **g**, *Shank3B*^{-/-} PSDs are thinner than wild-type PSDs. **h**, *Shank3B*^{-/-} PSDs are shorter than wild-type PSDs. **P* < 0.05, ***P* < 0.01, ****P* < 0.0001; two-way repeated measures ANOVA for **a**; two-tailed *t*-test for **b**, **c** and **e**; two-sample Kolmogorov-Smirnov test for **g** and **h**. Data in **g** and **h** are presented as cumulative frequency plot with histogram distribution and Gaussian curve fit for the insets. Data from **b**, **c** and **e** are presented as means ± s.e.m.; *n* = 36 from 3 wild-type mice and *n* = 36 from 3 *Shank3B*^{-/-} mice for **a**-**c**; *n* = 41 dendritic segments from 3 wild-type mice and *n* = 36 dendritic segments from 3 *Shank3B*^{-/-} mice for **e**; *n* = 144 PSDs from three wild-type mice and *n* = 140 PSDs from three *Shank3B*^{-/-} mice for **g**, **h**.

significant volumetric enlargement of this structure in *Shank3B*^{-/-} mice (Supplementary Fig. 9). These data suggest a correlation between neuronal hypertrophy and brain volume, consistent with studies from other mouse models of ASD^{22,23}.

Perturbation of striatal postsynaptic function

To elucidate the functional consequences of a disruption in *Shank3* on synaptic function, we performed recordings of cortico-striatal synaptic circuitry in acute brain slices of 6–7-week-old animals. We found that field population spikes were significantly reduced in *Shank3B*^{-/-} mice when compared with controls (Fig. 5a). Presynaptic function was not altered, as indicated by the relationship of stimulation intensity to the amplitude of the action potential component of the response termed negative peak 1 (NP1) and the paired-pulse ratio (PPR; Supplementary Fig. 10). These results indicate that the reduction in total field responses was most likely due to a postsynaptic impairment in synaptic function and/or a reduction in the number of functional synapses. Consistent with their mild behavioural phenotypes *Shank3A*^{-/-} mice displayed minimal disruption at cortico-striatal synapses (Supplementary Fig. 11).

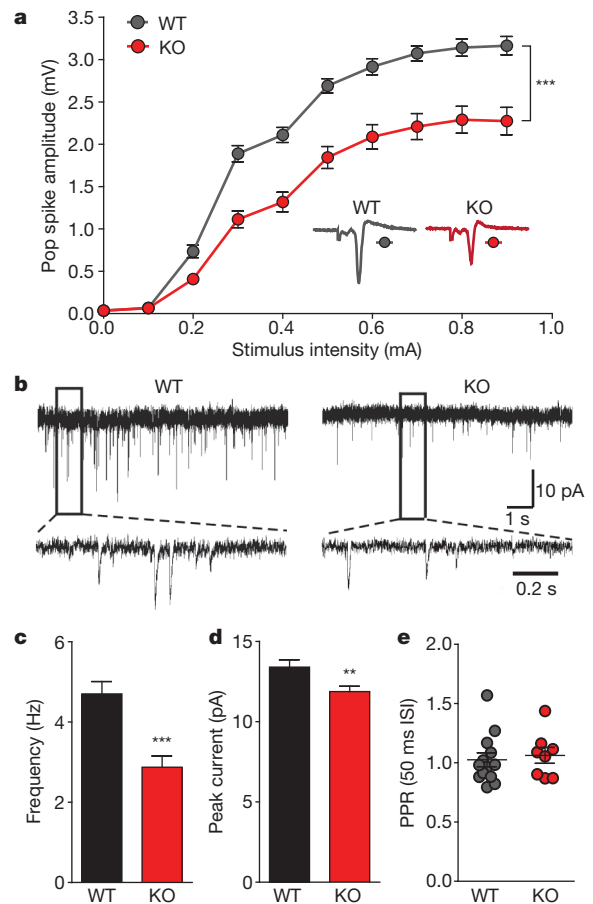


Figure 5 | Reduced cortico-striatal synaptic transmission in *Shank3B*^{-/-} MSNs. **a**, Cortico-striatal pop spike amplitude is decreased in *Shank3B*^{-/-} mice (red trace) as measured by extracellular field recordings. Inset, example traces for *Shank3B*^{-/-} (KO) and wild-type (WT). **b**, mEPSC example traces from wild-type and *Shank3B*^{-/-} MSNs recorded with whole-cell voltage clamp. **c**, **d**, Reduced mEPSC frequency (**c**) and amplitude (**d**) in *Shank3B*^{-/-} MSNs when compared to wild-type. **e**, PPR is unaltered in *Shank3B*^{-/-} MSNs. ***P* < 0.01, ****P* < 0.001; two-way repeated measures ANOVA, with Bonferroni post hoc test for **a**; two-tailed *t*-test for **c**, **d**; all data presented as means ± s.e.m. For field recordings, *n* = 13 slices from four mice per group; for mEPSCs, *n* = 29 MSNs from wild-type mice, *n* = 32 MSNs from *Shank3B*^{-/-} mice.

We next performed whole-cell voltage clamp recordings of α -amino-3-hydroxy-5-methyl-4-isoxazolepropionic acid receptor-miniature excitatory postsynaptic currents (AMPA-mEPSCs) in dorsolateral striatal MSNs. We found that the frequency of mEPSCs was significantly reduced in *Shank3B*^{-/-} MSNs (Fig. 5b, c), indicating a reduction in the number of functional synapses in *Shank3B*^{-/-} MSNs because we did not observe defects on presynaptic function by measuring PPR (Fig. 5e). We also found a significant reduction of peak mEPSC amplitude in *Shank3B*^{-/-} MSNs (Fig. 5b, d), indicating a reduction in the postsynaptic response from the available synapses. We did not observe significant differences in *N*-methyl-D-aspartate receptor (NMDA)/AMPA receptor-mediated current ratio in *Shank3B*^{-/-} neurons (Supplementary Fig. 12). Finally, similar defects in mEPSC frequency and amplitude were observed in *Shank3B*^{-/-} and wild-type littermate mice obtained from heterozygous matings (Supplementary Fig. 13). Together, these data demonstrate a critical role for SHANK3 in postsynaptic function in cortico-striatal circuitry.

To assess if the defects arising from *Shank3* dysfunction were specific to striatal circuitry or due to a more broad CNS perturbation, we performed a Morris water maze task for hippocampal-dependent learning and memory. We found that *Shank3B*^{-/-} mice performed at the same levels as controls in both learning and probe trials (Supplementary Fig. 14a–c). Reversal learning and probe trials again demonstrated similar levels of performance between *Shank3B*^{-/-} mice and controls (Supplementary Fig. 14d–f). Concomitantly, we performed electrophysiological recordings from the hippocampal CA1 sub-region and found no obvious difference in field recordings of population spikes or PPR between genotypes (Supplementary Fig. 15a–c). In addition, we found no significant differences in mEPSC frequency or mEPSC amplitude (Supplementary Fig. 15d–f). These data suggest that the observed behavioural and synaptic defects are specific to discrete brain regions and are not part of an overall CNS dysfunction.

Discussion

Despite recent advances in the understanding of autism spectrum disorder genetics, the underlying neurobiological substrates and neural circuits involved in these disorders remain largely unknown. The *Shank3* gene has become the focus of substantial interest, with an increasing body of evidences suggesting *Shank3* as the causative gene of the major neurological symptoms in the 22q13 deletion syndrome^{9,11–13,24}. Our present study with *Shank3* mutant mice not only sheds light on a critical *in vivo* role for SHANK3 in striatal glutamatergic synaptic structure and function, but also demonstrates causality between a disruption in this gene and the development of autistic-like behaviours in mice.

In this study, we generated two mutant alleles for the *Shank3* gene. These two lines of mice showed different levels of severity in synaptic defects and phenotypes. In humans, multiple mutations/variants of *Shank3* gene have been identified to coalesce at the ankyrin repeats and downstream of PDZ domain^{9,13}. Our data indicate that disruptions of different locations of the *Shank3* gene can lead to varying degrees of functional defects, which may in part contribute to phenotypic heterogeneity in *Shank3*-related ASDs. We should note that, in clinical conditions, the 22q13 deletions and the autism-associated *Shank3* mutations are heterozygous, whereas in our current study, we used homozygous mutant mice to get a clear understanding of the physiological role of the *Shank3* gene and the underlying functional consequences of its disruption. Further studies will be needed to elucidate potential functional deficits resulting from *Shank3* haploinsufficiency in *Shank3B*^{-/-} mice.

PSD-95–SAPAP–SHANK proteins form a key postsynaptic scaffold at glutamatergic synapses which interacts with many synaptic proteins, including the neuroligin–neurexin complex²⁵. In addition to *Shank3* (ref. 9), it is worth noting that *Shank2* (refs 6, 8), *SAPAP2* (ref. 6), neuroligin-1 (ref. 26) and neuroligin-3 and -4 (ref. 27) have all been

implicated in human ASDs. Therefore, the dysfunction of neuroligin–neurexin–PSD-95–SAPAP–SHANK complex could underlie a common synaptic mechanism for a subset of ASDs.

The precise circuitry defects involved in autistic behaviours are poorly understood. Neuroimaging studies provide evidence that caudate and frontal-striatal circuitries are dysfunctional areas in ASD^{28–30}. Cortico-striatal circuitry dysfunction has also been strongly implicated in repetitive/compulsive behaviours in obsessive-compulsive disorder (OCD)^{31–33}. We previously found that deletion of *SAPAP3*, which directly interacts with SHANK3 and is highly expressed in the striatum, leads to cortico-striatal circuitry dysfunction and OCD-like behaviours including repetitive/compulsive grooming in mice³¹. Repetitive behaviours are also often seen in autistic patients and in some mouse models of ASDs^{34–36}. SHANK3 is the most abundant SHANK family member expressed in the striatum and *Shank3B*^{-/-} mice exhibit excessive/repetitive grooming leading to skin lesions. Our data support the hypothesis that repetitive behaviours in OCD and ASD may share a common circuitry mechanism.

The regulation of social behaviours and social interaction is thought to be controlled by several brain regions and circuits³⁷. Similarly, genetic makeup is thought to have a key role in the phenotypic manifestation of social behaviours³⁸. The robust social interaction deficits in *Shank3B* mutant mice demonstrate a casual role for the disruption of this gene in the genesis of social dysfunction and provide a valuable experimental system for future genetic dissection of the neuronal basis of social behaviour.

METHODS SUMMARY

Behavioural analysis. Young adult mice 5–6-weeks old were used for all behavioural analyses except lesion scores which were performed in 4–5-month-old mice. All experiments were done blind to genotypes. All experimental procedures were reviewed and approved by the Duke University Institutional Animal Care and Use Committee and the MIT Committee on Animal Care.

Statistical analysis. Analyses were performed using Prism (GraphPad Software) and MATLAB (MathWorks). Details on particular tests used are described in the main text and in the methods section; a summary of statistical analysis for the behavioural data are presented in Supplementary Table 2.

Full Methods and any associated references are available in the online version of the paper at www.nature.com/nature.

Received 7 September 2010; accepted 22 February 2011.

Published online 20 March 2011.

1. American Psychiatric Association Task Force on DSM-IV. *Diagnostic and statistical manual of mental disorders: DSM-IV-TR* (American Psychiatric Association, 2000).
2. Rosenberg, R. E. *et al.* Characteristics and concordance of autism spectrum disorders among 277 twin pairs. *Arch. Pediatr. Adolesc. Med.* **163**, 907–914 (2009).
3. Abrahams, B. S. & Geschwind, D. H. Advances in autism genetics: on the threshold of a new neurobiology. *Nature Rev. Genet.* **9**, 341–355 (2008).
4. Bourgeron, T. A synaptic trek to autism. *Curr. Opin. Neurobiol.* **19**, 231–234 (2009).
5. Zoghbi, H. Y. Postnatal neurodevelopmental disorders: meeting at the synapse? *Science* **302**, 826–830 (2003).
6. Pinto, D. *et al.* Functional impact of global rare copy number variation in autism spectrum disorders. *Nature* **466**, 368–372 (2010).
7. Tabuchi, K. *et al.* A neuroligin-3 mutation implicated in autism increases inhibitory synaptic transmission in mice. *Science* **318**, 71–76 (2007).
8. Berkel, S. *et al.* Mutations in the SHANK2 synaptic scaffolding gene in autism spectrum disorder and mental retardation. *Nature Genet.* **42**, 489–491 (2010).
9. Durand, C. M. *et al.* Mutations in the gene encoding the synaptic scaffolding protein SHANK3 are associated with autism spectrum disorders. *Nature Genet.* **39**, 25–27 (2006).
10. Prasad, C. *et al.* Genetic evaluation of pervasive developmental disorders: the terminal 22q13 deletion syndrome may represent a recognizable phenotype. *Clin. Genet.* **57**, 103–109 (2000).
11. Wilson, H. L. *et al.* Molecular characterisation of the 22q13 deletion syndrome supports the role of haploinsufficiency of SHANK3/PROSAP2 in the major neurological symptoms. *J. Med. Genet.* **40**, 575–584 (2003).
12. Moessner, R. *et al.* Contribution of SHANK3 mutations to autism spectrum disorder. *Am. J. Hum. Genet.* **81**, 1289–1297 (2007).
13. Gauthier, J. *et al.* Novel de novo SHANK3 mutation in autistic patients. *Am. J. Med. Genet. B. Neuropsychiatr. Genet.* **150B**, 421–424 (2009).
14. Kim, E. *et al.* GKAP, a novel synaptic protein that interacts with the guanylate kinase-like domain of the PSD-95/SAP90 family of channel clustering molecules. *J. Cell Biol.* **136**, 669–678 (1997).

15. Takeuchi, M. *et al.* SAPAPs. A family of PSD-95/SAP90-associated proteins localized at postsynaptic density. *J. Biol. Chem.* **272**, 11943–11951 (1997).
16. Zoghbi, H. Y. & Warren, S. T. Neurogenetics: advancing the “next-generation” of brain research. *Neuron* **68**, 165–173 (2010).
17. Moy, S. S. *et al.* Sociability and preference for social novelty in five inbred strains: an approach to assess autistic-like behavior in mice. *Genes Brain Behav.* **3**, 287–302 (2004).
18. Hung, A. Y. *et al.* Smaller dendritic spines, weaker synaptic transmission, but enhanced spatial learning in mice lacking Shank1. *J. Neurosci.* **28**, 1697–1708 (2008).
19. Redcay, E. & Courchesne, E. When is the brain enlarged in autism? A meta-analysis of all brain size reports. *Biol. Psychiatry* **58**, 1–9 (2005).
20. Langen, M. *et al.* Changes in the developmental trajectories of striatum in autism. *Biol. Psychiatry* **66**, 327–333 (2009).
21. Hollander, E. *et al.* Striatal volume on magnetic resonance imaging and repetitive behaviors in autism. *Biol. Psychiatry* **58**, 226–232 (2005).
22. Bourgeron, T. A synaptic trek to autism. *Curr. Opin. Neurobiol.* **19**, 231–234 (2009).
23. Kwon, C. H. *et al.* Pten regulates neuronal arborization and social interaction in mice. *Neuron* **50**, 377–388 (2006).
24. Bonaglia, M. C. *et al.* Identification of a recurrent breakpoint within the SHANK3 gene in the 22q13.3 deletion syndrome. *J. Med. Genet.* **43**, 822–828 (2006).
25. Irie, M. *et al.* Binding of neuroligins to PSD-95. *Science* **277**, 1511–1515 (1997).
26. Kim, H. G. *et al.* Disruption of neurexin 1 associated with autism spectrum disorder. *Am. J. Hum. Genet.* **82**, 199–207 (2008).
27. Jamain, S. *et al.* Mutations of the X-linked genes encoding neuroligins NLGN3 and NLGN4 are associated with autism. *Nature Genet.* **34**, 27–29 (2003).
28. Silk, T. J. *et al.* Visuospatial processing and the function of prefrontal-parietal networks in autism spectrum disorders: a functional MRI study. *Am. J. Psychiatry* **163**, 1440–1443 (2006).
29. Horwitz, B., Rumsey, J. M., Grady, C. L. & Rapoport, S. I. The cerebral metabolic landscape in autism. Intercorrelations of regional glucose utilization. *Arch. Neurol.* **45**, 749–755 (1988).
30. Sears, L. L. *et al.* An MRI study of the basal ganglia in autism. *Prog. Neuropsychopharmacol. Biol. Psychiatry* **23**, 613–624 (1999).
31. Welch, J. M. *et al.* Cortico-striatal synaptic defects and OCD-like behaviours in Sapap3-mutant mice. *Nature* **448**, 894–900 (2007).
32. Shmelkov, S. V. *et al.* Slitrk5 deficiency impairs corticostriatal circuitry and leads to obsessive-compulsive-like behaviors in mice. *Nature Med.* **16**, 598–602 (2010).
33. Graybiel, A. M. Habits, rituals, and the evaluative brain. *Annu. Rev. Neurosci.* **31**, 359–387 (2008).
34. McFarlane, H. G. *et al.* Autism-like behavioral phenotypes in BTBR T+tf/J mice. *Genes Brain Behav.* **7**, 152–163 (2008).
35. Blundell, J. *et al.* Neuroligin-1 deletion results in impaired spatial memory and increased repetitive behavior. *J. Neurosci.* **30**, 2115–2129 (2010).
36. Etherton, M. R., Blaiss, C. A., Powell, C. M. & Sudhof, T. C. Mouse neurexin-1 α deletion causes correlated electrophysiological and behavioral changes consistent with cognitive impairments. *Proc. Natl Acad. Sci. USA* **106**, 17998–18003 (2009).
37. Insel, T. R. & Fernald, R. D. How the brain processes social information: searching for the social brain. *Annu. Rev. Neurosci.* **27**, 697–722 (2004).
38. Ebstein, R. P., Israel, S., Chew, S. H., Zhong, S. & Knafo, A. Genetics of human social behavior. *Neuron* **65**, 831–844 (2010).

Supplementary Information is linked to the online version of the paper at www.nature.com/nature.

Acknowledgements We thank C. Duarte, S. Chaterjee and A. Oliveira-Maia for discussions; L. Kruger and Q. Liu for technical assistance; A. Hadiono for assistance in behavioural annotation; D. Bredt for the PSD-93 antibody; T. Boeckers for the anti-SHANK3 antibody; S. Miller and P. Christopher for advice and assistance with electron microscopy techniques; J. Crawley for the demonstration of social behaviour tests; N. Calakos and Y. Wan for advice on electrophysiology studies; A. Graybiel for critical comments of the manuscript; D. Wang and the other members of the G.F. laboratory for their support. We thank The Poitras Center for Affective Disorders Research. This work was funded by a grant from NIMH/NIH (R01MH081201), a Hartwell Individual Biomedical Research Award from The Hartwell Foundation, and a Simons Foundation Autism Research Initiative (SFARI) grant Award to G.F.; a NARSAD Young Investigator Award and NIH Ruth L. Kirschstein National Research Service Award (F32MH084460) to J.T.T.; a NIH (R03MH085224) grant to Z.F.; and doctoral fellowships from the Portuguese Foundation for Science and Technology to J.P. (SFRH/BD/15231/2004) and C.F. (SFRH/BD/15855/2005). C.F. would like to acknowledge the support from the “Programa Gulbenkian de Doutoramento em Biomedicina” (PGDB, Oeiras, Portugal) and J.P. the “Programa Doutoral em Biologia Experimental e Biomedicina” (CNC, Coimbra, Portugal).

Author Contributions J.P., C.F., J.T.T., W.W., M.F.W., T.N.V., C.D.L. and Z.F. participated in the execution and analysis of experiments. J.P., C.F., J.T.T., C.D.L. Z.F. and G.F. participated in the interpretation of the results. J.P., C.F. and G.F. designed the experiments and wrote the paper.

Author Information Reprints and permissions information is available at www.nature.com/reprints. The authors declare no competing financial interests. Readers are welcome to comment on the online version of this article at www.nature.com/nature. Correspondence and requests for materials should be addressed to G.F. (fengg@mit.edu).

METHODS

Mice. *Shank3* mutant mice were generated by homologous recombination in R1 embryonic stem cells and implanted in C57 blastocysts using standard procedures. One targeting vector (Shank3A) was designed to replace exon 4–7 (containing the ankyrin repeat domains) and another vector (Shank3B) was designed to replace exon 13–16 (containing the PDZ domain) of the *Shank3* gene with a NEO cassette. Genotypes were determined by PCR of mouse tail DNA, using: for Shank3A, primer F1a (GGTTGAGGATGAGCAAGCTAG) and R1a (GGGACATAAGTGAAGGTTAGG) for the wild-type allele (318 base pairs), and F1a and R2 (TCAGGGTTATTGTCTCATGAGC; in the neo cassette) for the mutant allele (361 base pairs); for Shank3B, primer F1b (GAGCTCTACTCCCTT AGGACTT) and R1b (TCCCCCTTCACTGGACACCC) for the wild-type allele (316 base pairs), and F1b and R2 (TCAGGGTTATTGTCTCATGAGC; in the neo cassette) for the mutant allele (360 base pairs). The NEO cassette was not removed.

Chimaeric mice were crossed to C57 females (Jackson Labs). Initially, F1 hybrids from heterozygous \times heterozygous matings were generated. However, homozygous knockouts mice from this type of mating are smaller than their wild-type littermates, presumably due to an inadequate competition for resources during early postnatal days leading to different developmental trajectories. We postulated that this size difference would influence our behavioural tests. To alleviate this confound, heterozygous animals were crossed in direct brother-sister matings for five generations from which we derived F5 isogenic hybrids in a mixed background. These isogenic animals were then used to generate time-mated homozygous \times homozygous breeding pairs to obtain wild-type and mutant animals used in the experiments. F5 *Shank3A* and F5 *Shank3B* knockouts from these matings are reared to weaning age with weights similar to those from F5 control animals.

Animals were housed at a constant 23 °C in a 12 h light/dark cycle (lights off at 19:00), with food and water available *ad libitum*. Mice were housed 3–5 by genotype per cage with the exception of the animals individually housed for grooming measurements. Only aged-matched male mice were used for behavioural experiments, all other tests included age-matched males and females in proportional contribution across groups. Unless otherwise noted, all tests were conducted with naive cohorts of mice. All experimental procedures were reviewed and approved by the Duke University Institutional Animal Care and Use Committee and the MIT Committee on Animal Care.

Grooming behaviour³¹. Young adult male mice 5–6-week-old were used for analysis of grooming behaviour. Habituated, individually housed animals were video-taped for 24 h under 700 lx (day, 12 h) and ~2 lx (red light at night, 12 h) illumination. Grooming behaviours were coded from 19:00–21:00 h (that is, 2 h beginning at the initiation of the dark cycle); this segment was analysed using Noldus Observer software and the total amount of time in the 2-h segment spent grooming was determined. Grooming included all sequences of face-wiping, scratching/rubbing of head and ears, and full-body grooming. The observer was blinded to genotype during the scoring of the videotapes.

PSD preparation and western blot. PSD fractions of the striatum were prepared as previously described³¹, separated on SDS-PAGE and probed with specific antibodies. The relative amount of β -actin was used as loading control. Antibodies used in these experiments include rabbit antibodies against PSD-93 (gift from D. Bredt) and Shank3 (gift from T. Boeckers). The antibody for SAPAP3 has been previously described³⁹. Commercial antibodies used include monoclonal antibodies against NR1 (Transduction Laboratories), NR2B (Millipore), CaMKII (Transduction Laboratories), NR2A (Millipore), and β -actin (Sigma), as well as polyclonal antibodies against GluR1 (Abcam), Homer (Chemicon), GluR2 (Abcam), neuroligin-3 (Synaptic Systems) and PSD-95 (Abcam).

In situ hybridization. mRNA *in situ* hybridization was performed as described elsewhere³⁹. Briefly, reactions were performed with 20 μ m cryosections from freshly frozen 5-week-old brain mouse tissue using digoxigenin (DIG)-labelled riboprobes against mouse *Shank1* cDNA (NM_001034115; base pairs 4107–4924), *Shank2* cDNA (NM_001081370; base pairs 2063–2876) and *Shank3* (NM_021423; base pairs 3159–3959). The complementary DNAs used were all verified by sequencing compared to the following sequences GenBank accession numbers: (*Shank1*: NM_001034115), (*Shank2*: NM_001081370) and (*Shank3*: NM_021423). The hybridization signal was detected using an alkaline phosphatase (AP)-conjugated anti-DIG antibody (Roche) and developed using 5-bromo-4-chloro-indolylphosphate/nitroblue tetrazolium (BCIP/NBT; Roche).

Motor and anxiety-like behaviours³¹. **Zero maze:** an elevated zero maze was indirectly illuminated at 100 lx. Testing commenced with an animal being introduced into a closed area of the maze. Behaviour was video-taped for 5 min and subsequently scored by a trained observer using Noldus Observer software. Anxiety-like behaviour was deduced based upon the percent time spent in the open areas. The observer was blinded to genotype. The animals used in the zero

maze test, both *Shank3A*^{-/-}, *Shank3B*^{-/-} and respective controls were previously tested in the open field test with a 2-day period in between tasks.

Open field: spontaneous locomotor activity was evaluated over 30 min in an automated Omnitech Digiscan apparatus (AccuScan Instruments) as described³¹. Locomotor activity was assessed as total distance travelled (m). Anxiety-like behaviour was defined by number of rearings and time spent in the centre as compared to time spent in the perimeter (thigmotaxis) of the open field.

Dark-light emergence test: mice were habituated in an adjacent room to low light conditions (~40 lx) and the test room was initially under similar illumination. Testing was conducted in a two-chambered test apparatus (Med Associates), with one side draped in black cloth (that is, dark-chamber) and the other illuminated at ~1,000 lx (that is, light-chamber) with a high intensity house light and overhead fluorescent lamps. Upon placing the mice into the dark chamber, the light chamber was illuminated and the door between the two chambers was opened. The mice were allowed to freely explore the apparatus for 5 min. The latency to emerge from the darkened into the lighted chamber and the percentage of time spent in the illuminated chamber were used as indices of anxiety-like behaviours.

Social interaction paradigm. Three-chamber social test: sociability and response to social novelty test was performed as previously described¹⁷ with minor modifications. Briefly, 5–6-week-old male animals were used across all tests. Target subjects (Stranger 1 and Stranger 2) were 5–6-week-old males habituated to being placed inside wire cages for 5 days before beginning of testing. Test mice were habituated to the testing room for at least 45 min before the start of behavioural tasks. The social test apparatus consisted of a transparent acrylic box with removable floor and partitions dividing the box into three chambers. Here, the middle chamber (20 cm \times 17.5 cm) is half the width of Chamber 1 (20 cm \times 35 cm) and Chamber 2 (20 cm \times 35 cm) with the overall dimensions of the box being 60 cm (length) \times 35 cm (width) with 5 cm openings between each chamber which can be closed or open with a lever operated door. The wire cages used to contain the stranger mice were cylindrical, 11 cm in height, a bottom diameter of 10.5 cm with the bars spaced 1 cm apart (Galaxy Cup, Spectrum Diversified Designs). An inverted transparent cup was placed on the top of the cage to prevent the test mice from climbing on the top of the wire cage.

For the sociability test, the test animal was introduced to the middle chamber and left to habituate for 5 min, after which an unfamiliar mouse (Stranger 1) is introduced into a wire cage in one of the side-chambers and an empty wire cage on the other side-chamber. The dividers are then raised and the test animal is allowed to freely explore all three chambers over a 5 min session. Following the 5 min session, the animal remains in the chamber for an extra 5 min (post-test) to better acquire the identification cues from Stranger 1 animal. Following this, a novel stranger mouse (Stranger 2) is inserted in the wire cage previously empty and again the test animal is left to explore for a 5 min session. Time spent in each chamber, time spent in close proximity and heat maps were calculated using the automated software Noldus Ethovision. The release of the animals and relative position of social and inanimate targets was counterbalanced. However, for each individual test animal the location of Stranger 1 was maintained during Stranger 1 – E and Stranger 1 – Stranger 2 testing of the social behaviour.

Dyadic social interaction: animals were acclimatized to the test room for at least 1 h before the experiment. Target mice were wild-type and *Shank3B*^{-/-} of 6 weeks of age. Stimulus mice were conspecific age-matched wild-type mice socially naive to the target mice. At least 3 h before the beginning of the test, stimulus mice were given identifiable markings on the tails using a black marker pen. A pair of target and stimulus mice were introduced in a transparent Plexiglas arena (40 cm \times 40 cm \times 30 cm) covered with fresh bedding and the session recorded for 10 min. Quantification of social behaviours was performed using Noldus Observer software by a researcher blinded to the genotype of the target animals. Quantifications included: reciprocal social interaction, as determined by any sequence or combination of sequences involving close huddling, sniffing (for example, nose-to-nose, anogenital sniffing) or allogrooming by the target and stimulus mouse; the frequency of nose-to-nose sniffing; and the frequency of anogenital sniffing initiated by the target animal towards the stimulus mouse. Statistical tests were performed using unpaired two-tailed *t*-test.

Rotarod. Motor coordination was assessed in an accelerating rotarod test (4–40 r.p.m.). Briefly, animals were introduced in the apparatus (Med Associates) and the latency to fall was determined. Animals were tested for three trials in a single day with an inter-trial interval of 10 min.

Morris water maze. Morris water maze testing was conducted as describe elsewhere⁴⁰ with minor modifications. Male mice (4–5-weeks old) selected for the test were individually handled daily for 5 days before beginning the experiment. Testing pool was 120 cm in diameter and the platform 8 cm in diameter. The platform was submerged 1 cm below the water surface. Pool water was maintained at 23.0 \pm 0.5 °C and made opaque by mixing-in white non-toxic tempera paint. During training, 90 s duration trials were used, if the animals did not find

the platform within 90 s the experimenter guided the animal to the platform. After reaching the platform the animals were left for 15 s on top of the platform before being removed. Trials were administered for 5 days with four trials per animal per day with the platform located in the south-west quadrant. On the sixth day a 60 s probe trial was performed. On the seventh day, the reversal training commenced with the platform in the north-east quadrant, and proceeded as described above. The experimenter followed the animals' progress using tracking software outside of the testing room. Tracking and analysis were performed using the Noldus Ethovision software.

Golgi staining and Sholl analysis. All brains and collected sections were coded in order to blind the experimenter of the genotype until after all data was collected and analysed. Brains from 5-week-old, gender-matched *Shank3B*^{-/-} and control mice were prepared using standard Golgi-Cox impregnation technique using the FD Rapid GolgiStain Kit (NeuroTechnologies). Serial coronal sections of 100 μ m were collected from controls and *Shank3B* mutant animals. A total of 12 cells per animal were traced across the dorsal striatum as to sample representatively from this structure for a final number of 36 cells per genotype. For each animal, sections were selected to be between rostral-caudal bregma 1.18 mm and 0.86 mm. Criteria to identify medium spiny neurons were, (1) presence within the caudate putamen; (2) full impregnation of the neuron along the entire length of the dendritic arborization; (3) relative non-overlap with surrounding neurons and isolation from astrocytes and blood vessels and (4) morphologically, by the presence of high number of spines and relatively short neuronal arborizations as characteristics of MSNs. For each selected neuron the entire neuronal arbor was reconstructed under a $\times 100$ oil lens in a motorized microscope with a digital CCD camera connected to a computer running NeuroLucida Software (MBF Bioscience). The three-dimensional analysis of the reconstructed neurons was performed using NeuroExplorer software (MBF Bioscience) and data from branch length, number of branches and neuronal complexity was measured and analysed in Prism (Graph Pad). Two-way repeated measures ANOVA was used for Sholl analysis. Statistical significance was accepted when $*P < 0.05$, $**P < 0.01$ and $***P < 0.0001$.

Cortico-striatal electrophysiology. Brain slice preparation for extracellular field recording: acute brain slices were prepared from 6–7-week-old mice. Slices were prepared from one WT and one KO pair each day and the experimenter was blinded to the genotype. The mice were deeply anesthetized by intra-peritoneal injection of avertin and then transcardially perfused with carbogenated (95% O₂, 5% CO₂) ice-cold protective cutting artificial cerebrospinal fluid (aCSF) with the composition (in mM): 119 glycerol, 2.5 KCl, 1.25 NaH₂PO₄, 26 NaHCO₃, 25 glucose, 2 thiourea, 5 L-ascorbic acid, 3 Na-pyruvate, 0.5 CaCl₂·4H₂O, 10 MgSO₄·7H₂O. Mice were then decapitated and the brains were removed into ice-cold cutting solution for an additional 1 min. The brains were then rapidly blocked for coronal sectioning at 300- μ m thickness on a VF200 model compresstome (Precisionary Instruments) using either a sapphire or zirconium ceramic injector style blade. Slices containing the dorsal striatum were initially recovered for 30 min at room temperature (23–25 °C) in a carbogenated protective recovery aCSF (same composition as the cutting aCSF except that glycerol was replaced with *N*-methyl-D-glucamine (NMDG)-Cl as a substitute for NaCl to prevent initial excitotoxic swelling during re-warming). After this initial 30 min period the slices were transferred into a holding chamber containing carbogenated normal aCSF of the composition (in mM): 119 NaCl, 2.5 KCl, 1.25 NaH₂PO₄, 26 NaHCO₃, 12.5 glucose, 2 CaCl₂·4H₂O, 1 MgSO₄·7H₂O. The holding aCSF was supplemented with (in mM): 2 thiourea, 1 L-ascorbic acid, 3 Na-pyruvate to improve slice health and longevity, and slices were stored for 1–6 h before transfer to the recording chamber for use. The osmolarity of all solutions was measured at 300–310 mOsm and the pH was maintained at ~ 7.3 after equilibration under constant carbogenation.

Supplementary Fig. 11 shows summary data for corticostriatal field recordings from acute coronal brain slices of *Shank3A* mutant versus WT mice. The method of slice preparation differed significantly in these earlier experiments. Mice were transcardially perfused with carbogenated ice-cold protective sucrose aCSF with the composition (in mM): 185 sucrose, 2.5 KCl, 1.25 NaH₂PO₄, 26 NaHCO₃, 25 glucose, 0.5 CaCl₂·4H₂O, 4 MgSO₄·7H₂O (pH 7.3, 300–310 mOsm) without supplementation of antioxidants. Slices were immediately transferred into a holding chamber containing carbogenated normal aCSF of the composition (in mM): 119 NaCl, 2.5 KCl, 1.25 NaH₂PO₄, 26 NaHCO₃, 12.5 glucose, 2 CaCl₂·4H₂O, 1 MgSO₄·7H₂O (pH 7.3, 300–310 mOsm) without supplementation of antioxidants, and slices were stored for 1–4 h before transfer to the recording chamber. The absence of the initial 30 min recovery period in 'protective' aCSF in addition to the absence of antioxidant supplementation in the cutting aCSF and in the aCSF in the holding chamber results in more rapid deterioration of slice health and smaller evoked population spike amplitudes on average, indicating reduced overall slice viability compared to slices prepared with a 30 min NMDG aCSF recovery protocol described above. However, WT and KO brain slices were

always subjected to identical procedures on any given day of recording and the procedures were always standardized for each discrete experimental data set so that these factors would not introduce any potential confounds.

Extracellular field recording. A platinum iridium concentric bipolar stimulating electrode (CBAPC75, 25 μ m inner pole diameter; FHC) was placed on the inner border of the corpus callosum between the cortex and dorsolateral striatum. This electrode position was chosen to predominantly activate cortical axons within the corpus callosum which heavily converge upon striatal MSNs to form excitatory corticostriatal synaptic connections. Although there is ample evidence on which to base our assertion that stimulation of the corpus callosum predominantly results in activation of cortical axons^{41,42}, we are unable to exclude the possibility of a relatively smaller contribution arising from activation of thalamostriatal axons that have distal terminals in dorsolateral striatum nearby to the stimulated region. Thus, although we refer to our measurements as primarily reflecting corticostriatal transmission, our measurements are not 'pure' corticostriatal responses. Borosilicate glass recording electrodes filled with 2 M NaCl were placed in the dorsolateral striatum approximately 400–450 μ m away from the stimulating electrode. Corticostriatal field population spikes were evoked with 0.15 ms step depolarizations at 0.5 mA intensity at a frequency of 0.05–0.1 Hz. Paired pulses were evoked with a 100 ms inter-stimulus interval. Baseline responses were monitored to ensure stable population spike amplitude for a minimum of 5 min. Input-output functions were then determined for the negative peak 1 (NP1; presynaptic fibre volley) and population spike amplitude by three consecutive rounds of stimulation from 0–1.0 mA in 0.1 mA increments. All recordings were performed at room temperature and acquired using pCLAMP 10 software (Axon Instruments/Molecular Devices). Data analysis was performed blind to genotype in Clamp fit (Axon Instruments/Molecular Devices). Population spike amplitude was measured as the average of the early peak positivity to the peak negativity and from the peak negativity to the late peak positivity. This standard method takes into account the fact that the downward population spike is superimposed on an upward field excitatory postsynaptic potential (fEPSP). Paired pulse ratio (PPR) was calculated as the ratio of the 2nd population spike amplitude to the 1st population spike amplitude for responses to paired pulse stimulation at 0.5 mA fixed intensity with a 100 ms inter-stimulus interval for the pair.

Extracellular field recordings and whole-cell mEPSC recordings in the hippocampal CA1 region were conducted in 300 μ m thick acute brain slices from 6–9-week-old WT and *Shank3B* mutant mice. For measurement of hippocampal CA1 population spikes, a concentric bipolar stimulating electrode was placed in the striatum radiatum to stimulate the Schaffer collateral pathway, and a borosilicate glass recording electrode (~ 2 – 3 M Ω) filled with recording aCSF was placed in the CA1 pyramidal cell layer approximately 400 μ m from the stimulation site. The recording electrode was placed at the depth in the slice that gave the largest population spike amplitude, and a stable baseline was established for < 10 min. Input-output recordings were conducted by increasing the stimulation intensity from 0 to 160 μ A in 20 μ A increments. Three successive rounds were collected and values at each intensity represent the average of the three measurements. CA1 population spike amplitude was quantified exactly as described previously for cortico-striatal population spikes. For CA1 pyramidal neuron whole-cell recordings, pyramidal neurons in CA1 were identified under infrared-differential interference contrast (IR-DIC) visualization. Cells were patched with a Caesium-gluconate-based internal solution containing (in mM): 110 Caesium-gluconate, 15 KCl, 4 NaCl, 5 TEA-Cl, 20 HEPES, 0.2 EGTA, 5 lidocaine *N*-ethyl chloride, 4 ATP magnesium salt, and 0.3 GTP sodium salt. The pH was adjusted to 7.25 with D-gluconic acid and osmolarity was adjusted to 290–300 mOsm with sucrose as necessary. The recording aCSF contained 1 μ M TTX, 100 μ M picrotoxin, 5 μ M CGP55845, and 50 μ M D-APV to isolate pure AMPAR-mediated mEPSCs. CA1 neurons were voltage-clamped at -80 mV to amplify the smallest spontaneous miniature synaptic events that might otherwise escape detection. Criteria for acceptance were uncompensated stable $R_{in} < 25$ M Ω and holding current < -300 pA. mEPSCs were detected using MiniAnalysis software (Synaptosoft) as described for striatal MSNs. All recordings were carried out at room temperature (23–25 °C). Slices were prepared in a 20–30 degree off-horizontal cutting angle (optimal for CA1 region) from one WT and one KO pair each day and the experimenter was blind to the genotypes of the animals.

Striatal slice preparation for whole-cell recording. Mice 5–6-week-old were used for all whole-cell electrophysiology procedures by an experimentalist blinded to genotype. Acute coronal striatal slices were prepared as follows. Briefly, mice were anesthetized with Avertin solution (20 mg/ml, 0.5 mg/g body weight) and perfused through the heart with a small volume (about 20 ml) of ice-cold and oxygenated (95% O₂, 5% CO₂) cutting solution containing (mM): 105 NMDG, 105 HCl, 2.5 KCl, 1.2 NaH₂PO₄, 26 NaHCO₃, 25 Glucose, 10 MgSO₄, 0.5 CaCl₂, 5 L-Ascorbic Acid, 3 Sodium Pyruvate, 2 Thiourea (pH 7.4, with osmolarity of 295–305 mOsm). The brains were rapidly removed and placed in ice-cold and oxygenated cutting solution. The coronal slices (300 μ m) were prepared

using a slicer (Vibratome 1000 Plus, Leica Microsystems, USA) and then transferred to an incubation chamber (BSK4, Scientific System Design Inc., USA) at 32 °C with carbogenated cutting solution, which was gradually replaced with aCSF in 30 min through a peristaltic pump (Rainin, RP-1) allowing a precise regulation of flowing rates. The slices were then kept in the aCSF that contained (mM): 119 NaCl, 2.3 KCl, 1.0 NaH₂PO₄, 26 NaHCO₃, 11 Glucose, 1.3 MgSO₄, 2.5 CaCl₂ (pH was adjusted to 7.4 with HCl, with osmolarity of 295–305 mOsm) at room temperature for at least 30 min.

Whole-cell patch-clamp. The slice was placed in a recording chamber (RC-27L, Warner Instruments) and constantly perfused with oxygenated aCSF at 24 °C (TC-324B, Warner Instruments) at a rate of 1.5–2.0 ml min⁻¹. The striatum and individual MSNs were visualized and identified with a microscope equipped with IR-DIC optics (BX-51WI, Olympus) by location, shape and size (ovoid cell body with major axis of 10 to 14 μm). Two additional measures were used to distinguish them from similar sized GABAergic interneurons. First, GABAergic interneurons show smaller membrane capacitance (C_m) and membrane time constant (τ_m) (at least two times less) when compared to that of MSNs. In the case of recordings done with Cs⁺ internal, these membrane properties were measured immediately after membrane rupture when the Cs⁺ internal has not been dialysed and taken effect yet. Second, AMPA receptor-mediated mEPSCs showed much faster kinetics (including both rise time and decay time constant, τ decay) in GABAergic interneurons. Whole-cell patch-clamp recordings were obtained from MSNs using recording pipettes (King Precision Glass, glass type 8250) pulled in a horizontal pipette puller (P-87, Sutter Instruments) to a resistance of 3–4 MΩ, when filled with the internal solution containing (in mM): 107 CsMeSO₃, 10 CsCl, 3.7 NaCl, 5 TEA-Cl, 20 HEPES, 0.2 EGTA, 5 lidocaine *N*-ethyl chloride, 4 ATP magnesium salt, and 0.3 GTP sodium salt. pH was adjusted to 7.3 with KOH and osmolarity was adjusted to 298–300 mOsm with 15 mM K₂SO₄.

To record AMPA receptor-miniature excitatory postsynaptic currents (mEPSCs), the cells were held in voltage clamp at -70 mV in the presence of 50 μM APV (DL-2-amino-5-phosphono-valeric acid), 25 μM BMR (1(S),9(R)-(-)-bicuculline methiodide), 10 μM D-serine and 1 μM TTX (all from Tocris). The miniature events were not recorded until 5 min after entering whole cell patch clamp recording mode to allow the dialysis of Cs⁺ internal solution for a relatively complete block of the potassium channels in the MSNs. The mEPSCs were detected and analysed with MiniAnalysis (Synaptosoft).

For paired-pulse stimulation experiments, AMPAR mediated excitatory postsynaptic currents (EPSCs) were evoked by a local concentric bipolar stimulating electrode (CBARC75, FHC) that was placed in the inner edge of corpus callosum within the dorso-lateral region of the striatum. Recordings were made in the presence of picrotoxin (100 μM) and APV (50 μM) to block activation of GABA_A receptors and NMDA receptors. Stimulation was current-controlled (ISO-Flex, A.M.P.I.). The stimulus intensity was set at a level that could evoke 300–400 pA AMPAR-mediated response for all the cells measured and delivered with an inter-stimulus interval of 50 ms. The paired-pulse measurements were obtained for 15–20 consecutive traces and only those traces with stable evoked first current response were used for data analysis. The PPR was calculated with the peak current response to the second pulse divided by that of the first response.

NMDAR- and AMPAR- mediated synaptic current ratio (NMDA/AMPA ratio) was recorded in the presence of picrotoxin at holding potentials of +40 mV and -70 mV, respectively. The NMDA/AMPA ratios were measured according to previously described methods⁴³. Briefly, the stimulus intensity was set at a level that could evoke 300–400 pA AMPAR-mediated response with a holding potential at -70 mV. Each evoked response was repeated for 15–20 times with an inter-stimulus interval of 20 s for all the cells measured. The time point of the peak current at -70 mV, considered to be fully mediated by AMPARs, was used to establish the time window for measuring the AMPA peak at +40 mV. The decay to baseline of the AMPA current at -70 mV was used to select a time window for measurement of the NMDA current; a 10-ms measurement window beginning 40 ms after the stimulus artefact was used. This current amplitude at this point was designated as the NMDAR mediated synaptic current response. (I_{NMDA} at +40 mV/ I_{AMPA} at -70 mV) was taken as the NMDA/AMPA ratio.

Data acquisition and analysis. A Multiclamp 700B amplifier (Molecular Devices Corporation) and digidata 1440A were used to acquire whole cell signals. The signals were acquired at 20 kHz and filtered at 2 kHz. The series-resistance was <20 MΩ. Values are expressed as means ± s.e.m. Data were tested for significance using either an unpaired *t*-test or a two-way repeated measures ANOVA.

Cell filling. Mice were assigned a code previous to dissection, as to maintain a blinded genotype across all procedures, including dissection, cell filling, imaging and quantification. Mice were deeply anesthetized with an overdose of isoflurane and transcardially perfused with PBS (pH 7.4) followed by ice-cold 4% paraformaldehyde/PBS (PFA) (pH 7.4). The brains were removed and post-fixed

overnight in PFA 4%. After post-fixation, the brain was sliced at 200-μm thickness coronal sections in a vibratome and kept in PBS at 4 °C. For cell filling injections, selected brain slices immersed in PBS were mounted in a tissue stage. Dorsal striatal medium cells were targeted with post hoc confirmation of being medium spiny neurons (morphology and spine density). Using a micromanipulator, micropipettes loaded with Lucifer Yellow dye (Sigma L-0259, 8% solution in 0.05 M Tris buffer, pH 7.4) were used to impale the cell body. A micropipette containing a solution of 0.1 M LiCl was used to deliver the dye with a continuous 10 nA current for 5 min. Following cell filling, a post-staining was used to amplify the fluorescent signal. Briefly, sections were transferred to blocking solution (5% sucrose, 2% BSA, and 1% Triton X-100 in PBS) containing 1:500 rabbit anti-Lucifer Yellow antibody (Invitrogen A5750) and incubated gently for 3 days at 4 °C. Sections were washed three times for 5 min in blocking solution and incubated 2 h at room temperature with 1:400 biotinylated goat anti-rabbit antibody (Vector Laboratories BA-1000). Next, sections were washed three times for 5 min in PBS. A tertiary incubation was performed by incubating sections for 2 h at room temperature in streptavidin-conjugated Alexa 488 (Invitrogen S11223) diluted 1:1,000 in PBS. Finally, sections were washed three times in PBS, mounted on slides using Fluoro-Gel (EMS, 17985-10) and imaged by confocal microscopy. Spine density was calculated automatically using NeuronStudio (Mount Sinai School of Medicine) and manually curated by an observer using a three-dimensional analysis of the dendritic image stack. All spine counts began 30 μm away from the outer edge of the soma and extended for an additional 10–60 μm away from the starting point. The data from spine density passed the Lilliefors normality test and D'Agostino & Pearson omnibus normality test. Spine metrics relating to spine length, spine neck diameter and spine neck width were collected using ImageJ (NIH). All analyses of spine metrics were performed by observers that were blinded to the genotypes of the animals.

Electron microscopy. Mice were assigned a code previous to dissection, as to maintain a blinded genotype across all procedures, including dissection, sample processing, imaging and quantification. Mice were deeply anesthetized with an overdose of isoflurane and transcardially perfused with PBS (pH 7.4) followed by ice-cold 4% paraformaldehyde (PFA) in phosphate buffer (pH 7.4). The brains were removed, the striatum dissected and post-fixed overnight in PFA 4%, then transferred into a 4% glutaraldehyde solution and kept at 4 °C for 3 days. The samples were washed twice, 20 min each, in 7.5% sucrose, 0.1 M sodium cacodylate buffer, then post-fixed in 1% osmium tetroxide for 2 h with initial microwave treatment for 6 min. Next, the samples were washed twice in 0.11 M veronal acetate buffer for 20 min each. Following en-block staining in 1% uranyl acetate in distilled water for 1 h the samples were washed twice in 0.11 M veronal acetate buffer for 20 min each. Samples were dehydrated using serial dilutions of ethanol (70%, 95%, 2 × 100%) for 20 min each, with initial microwave treatment of 2 min. Samples were then treated for 20 min twice with propaline oxide and impregnated with 50:50 propaline oxide:Epon resin overnight at 4 °C, with initial microwave treatment for 3 min. Next, the samples were impregnated with 100% Epon resin, three changes of 2 h each, with initial microwave treatment for 3 min each. Tissue samples were embedded in moulds and incubated for 48 h at 60 °C. Afterwards, semi-thin sections (0.5 μm) were cut on a Leica UltraCut S ultramicrotome and stained with Toluidine (0.8%) stain. From these, thin striatal sections (70 nm) were cut on an UltraCut S, mounted on 200 mesh Metaxaform Copper Rhodium grids and post-stained in 2% uranyl acetate in distilled water for 15 min and Sato's Lead citrate stain for 7 min. Grids were examined on a Philips (FEI) CM 12 transmission electron microscope. Images were acquired at ×40,000 magnification using an AMT 2Vue system, with an ORCA HR High resolution digital camera 7 megapixels, a Hamamatsu DCAM board for acquisition and AMT Image Capture Engine software version 600.335f. Images were saved as 7.5 megapixels 8 bit TIFF format files. PSD measurements were performed using ImageJ (NIH) by an observer that was blinded to the genotype of the samples.

Magnetic resonance image acquisition. Animals were assigned a blinding code, which was maintained during magnetic resonance (MR) data acquisition and analysis. MR mouse brain imaging was performed on a 7T Bruker Biospec 70/30 horizontal bore system (Billerica). Animals were lightly anesthetized under isoflurane with continuous monitoring and maintenance of physiological parameters throughout the imaging session (~60 min for each animal). Axial two-dimensional T2-weighted fast spin echo images (TURBO-RARE, TE/TR = 11/4,200 ms with 1 mm slice thick, matrix = 256 × 256 and FOV of 2.4 cm × 2.4 cm, five averages, 0.0 mm interslice gap) images were first obtained for screening purposes and supplemental anatomic information. For directed striatal and brain volumetric analysis, 64 contiguous 500-μm thick three-dimensional FSE proton density images (TURBO-RARE, TE/TR = 9/1,500 ms, matrix = 256 × 256 × 64 and FOV 2.2 cm × 2.2 cm × 2.2 cm, 25 min duration) were acquired.

MR volumetry measurements. Volumetric analysis of MR data sets was performed in OsiriX software, an open source image processing application

developed and maintained by Pixmeo. The left caudate-putamen was manually segmented in each animal by an investigator blinded to genotype. Each caudate-putamen was traced on contiguous axial slices from the three-dimensional volume acquisition with reference to a high-resolution age-matched mouse brain atlas (The Mouse Brain Atlas, The Mouse Brain Library at <http://www.mbl.org>). Selected areas were reviewed for consistency on coronal and sagittal representations, and cross-correlated with axial two-dimensional FSE images. Volumes were computed within OsiriX. Two separate striatal segmentations were obtained for each animal, with the average volume then taken. Intrarater reliability (kappa value) was = 0.97.

Volume normalization. Unilateral caudate-putamen volumes were normalized to brain volume measurements obtained from the same three-dimensional volume sets. Because of susceptibility distortions within the posterior fossa, and variable inclusion from animal to animal of posterior fossa contents at the caudal end of the 64 slice three-dimensional volume set, 'whole' brain volumes for normalization were obtained in each animal from traces beginning rostrally at the

olfactory bulbs and ending caudally through the cerebral aqueduct at the roof of the fourth ventricle. As with striatal volumes, brain volumes were computed in OsiriX from the average of two segmentations. Intrarater reliability (kappa value) was >0.99. Statistical analysis was performed with unpaired two-tailed *t*-test.

39. Welch, J. M., Wang, D. & Feng, G. Differential mRNA expression and protein localization of the SAP90/PSD-95-associated proteins (SAPAPs) in the nervous system of the mouse. *J. Comp. Neurol.* **472**, 24–39 (2004).
40. Vorhees, C. V. & Williams, M. T. Morris water maze: procedures for assessing spatial and related forms of learning and memory. *Nature Protocols* **1**, 848–858 (2006).
41. Yin, H. H., Davis, M. I., Ronesi, J. A. & Lovinger, D. M. The role of protein synthesis in striatal long-term depression. *J. Neurosci.* **26**, 11811–11820 (2006).
42. Malenka, R. C. & Kocsis, J. D. Presynaptic actions of carbachol and adenosine on corticostriatal synaptic transmission studied *in vitro*. *J. Neurosci.* **8**, 3750–3756 (1988).
43. Myme, C. I., Sugino, K., Turrigiano, G. G. & Nelson, S. B. The NMDA-to-AMPA ratio at synapses onto layer 2/3 pyramidal neurons is conserved across prefrontal and visual cortices. *J. Neurophysiol.* **90**, 771–779 (2003).